Divergent synthesis routes and superconductivity of ternary hydride $MgSiH_6$ at high pressure

Yanbin Ma,[1] Defang Duan,[1] Ziji Shao,[1] Hongyu Yu,[1] Hanyu Liu,[2] Fubo Tian,[1] Xiaoli Huang,[1] Da Li,[1] Bingbing Liu,[1] and Tian Cui[1,*]

[1]*State Key Laboratory of Superhard Materials, College of Physics, Jilin University, Changchun 130012, People's Republic of China*

[2]*Geophysical Laboratory, Carnegie Institution of Washington, Washington, DC 20015, USA*

(Received 20 July 2017; revised manuscript received 15 October 2017; published 31 October 2017)

We predict a new ternary hydride $MgSiH_6$ under high pressures, which is a metal with an ionic feature and takes on a simple cubic structure with space group Pm-3 above 250 GPa. Our first-principles calculations show that the cubic $MgSiH_6$ is a potential high-temperature superconductor with a superconducting transition temperature T_c of $\sim$ 63 K at 250 GPa. Further analysis suggests that phonon softening along mainly Γ-X and Γ-M directions induced by Fermi surface nesting plays a crucial role in the high-temperature superconductivity. Herein we propose the "triangle straight-line method" which provides a clear guide to determine the specific A + B $\rightarrow$ D type formation routes for ternary hydrides of the Mg-Si-H system and it effectively reveals two divergent paths to obtain $MgSiH_6$ under high pressures: $MgH_2 + SiH_4 \rightarrow MgSiH_6$ and $MgSi + 3H_2 \rightarrow MgSiH_6$. This method might be applicable to all ternary compounds, which will be very significant for further experimental synthesis.

DOI: 10.1103/PhysRevB.96.144518

I. INTRODUCTION

An excitingly theoretical prediction [1] and experimental observations [2,3] of superconductivity in strongly squeezed solid hydrogen sulfide with a high superconducting transition temperature T_c of $\sim$200 K have been widely recognized as one of the most significant findings in the superconducting field. What is more, these breakthrough discoveries reignite interest in seeking possible high temperature superconductors in other hydrogen-dominated compounds. Thus far, a large number of researches are mainly focused on binary hydrides and extensive investigations suggest that high T_c usually involves a large hydrogen framework [4]. In these binary hydrogen-rich high-T_c superconductors, doped elements play a role to metallize hydrogen at lower pressures, which is defined as so-called "chemical precompression" [5], but in fact, hydrogen is mainly responsible for the superconductivity owing to its light atomic mass and high Debye temperature. Based on this essence, some ternary hydrogen storage materials are believed to be candidates as high-temperature superconductors.

Experimentally, Muramatsu *et al.* found that the ternary $BaReH_9$ transforms into a superconductor with T_c of $\sim$7 K above 100 GPa [6]. Theoretically, the $Cmc2_1$ phase of Fe_2SH_3 was predicted to be stable at 100 GPa, but its electron phonon coupling (EPC) parameter λ is just 0.30 and that results in a fairly low $T_c = 0.3$ K at 173 GPa [7]. Recently, Rahm *et al.* predicted that $P4/mmm$-$KAuH_2$, $I4$-$Ba(AuH_2)_2$, and $I4$-$Sr(AuH_2)_2$, which contain AuH_2^- molecular units, are superconductors with T_c of 0.3, 30, and 10 K at 120 GPa, 1 atm, and 1 atm, respectively [8]. Earlier, a CH_4 molecular unit was found in ternary superconductive $P4/nmm$-$MgCH_4$ at high pressures [9].

Silicon (Si) is the next group-IVA element isoelectronic to C. Undoubtedly, someone may argue that a Si atom would bond with four H atoms to form SiH_4 molecular units in a Mg-Si-H system similar to $MgCH_4$. However, owing to the larger atomic core of Si than those of C, Si-H bonding is expected to be weaker than that of C-H, which might promote the dissociation of the Si-H bonding and then lead to some completely different crystal structures and novel properties at high pressure. Similarly, a typical example is a MH_4 (M = Si [10], Ge [11], and Sn [12]) system, where the discrepancies of bonding render substantially different structures and properties.

In addition, high pressure can stabilize some novel and unexpected stoichiometric binary hydrides. For instance, NaH_3, NaH_7, and possible NaH_9 were reported to be synthesized by compressing NaH and H_2 [13]. More intriguingly, our group proposed three different paths to obtain solid H_3S [14], i.e., $2H_2S + H_2 \rightarrow 2H_3S$, $3H_2S \rightarrow 2H_3S + S$, and $3H_2 + 2S \rightarrow 2H_3S$. Strobel *et al.* have reported that $(H_2S)_2H_2$ (stoichiometric H_3S) can be formed by mixing hydrogen sulfide (H_2S) and hydrogen (H_2) at high pressure [15]. Theoretical predictions proposed the H_3S could be the high-pressure decomposition product of H_2S [14,16,17], which has been confirmed by synchrotron x-ray diffraction experiment [3]. More recently, H_3S was directly synthesized by combining molecular hydrogen (H_2) with sulfur (S) at about 50 GPa [18].

Likewise, pressure could also synthesize some unusual ternary hydrides in the Mg-Si-H system. Nevertheless, how to determine synthesis paths for these stable ternary hydrides will be critical because of these rich precursors (e.g., Mg, Si, H_2, MgH_2, SiH_4, etc.). Once these synthetic paths are identified, they will be very helpful in stimulating further experimental synthesis. In this work, we proposed a method to determine an A + B $\rightarrow$ D (reactants A, B and resultant D) type high-pressure formation route. Moreover, we predicted that the cubic $MgSiH_6$ (group space Pm-3) has a high T_c of 63 K at 250 GPa and soft phonon modes play a significant role in superconductivity.

II. COMPUTATIONAL METHODS AND DETAILS

We explored these stoichiometries and crystal structures of the Mg-Si-H system at the pressure range of 50–300 GPa

*Corresponding author: cuitian@jlu.edu.cn

by means of an evolutionary algorithm and a particle swarm optimization algorithm, implemented in the USPEX (Universal Structure Predictor: Evolutionary Xtallography) [19,20] and CALYPSO (Crystal structure AnaLYsis by Particle Swarm Optimization) code [21,22], respectively. Both of two methods are very successful in predicting ternary high-pressure crystalline structures [7,23–25]. Unlike binary compounds, too many structures and stoichiometries need to be considered in complicated ternary hydrides. Therefore, we employed a variable-composition prediction method in USPEX to seek possible stoichiometries. Subsequently, we further used CALYPSO and USPEX to research these structures of possible stoichiometries with 1–4 formula units.

Structural relaxations and calculations of electronic properties were carried out by using the projector augmented-wave potentials [26] implemented in the Vienna *ab initio* simulation VASP code [27]. $1s$, $3s^2$, and $3s^2\,3p^2$ configurations were treated as valence electrons for H, Mg, and Si, respectively. The exchange-correlation functional was described by adopting the generalized gradient approximation (GGA) of Perdew-Burke-Ernzerhof (PBE) [28]. For structural searches, a kinetic cutoff energy of 500 eV and Monkhorst-Pack k meshes with grid spacing $2\pi\times0.05$ Å^{-1} were found to be sufficient. Furthermore, these selected structures were reoptimized by employing a more precise set of parameters: a basis set cutoff of 1000 eV and a k-point grid spacing of $2\pi\times0.03$ Å^{-1}. The high precision parameters ensure the enthalpy converges better than 1 meV/atom. The zero-point energy (ZPE) is calculated by using VASP in conjunction with the PHONOPY code [29] with $3\times3\times3$ supercells.

Phonon and incipient electron-phonon coupling (EPC) calculations were performed based on density functional perturbation theory (DFPT) [30] through the Quantum-ESPRESSO code [31]. The generalized gradient approximation correction (GGA) of PBE within norm-conserving pseudopotentials of Troullier-Martins (TM) form [32] was tested to be used. The kinetic energy cutoff and the charge density cutoff of the plane wave basis were chosen to be 100 and 400 Ry, respectively. Self-consistent electron density was evaluated by employing $24\times24\times24$ k mesh. Both phonon and EPC were calculated by using a $6\times6\times6$ q mesh.

Subsequently, considering the effect of Brillouin zone sampling to EPC [33–35], we further used a recently developed Wannier interpolation method [36] to recalculate the EPC with fine k and q grids. In the Wannier interpolation calculation, we used the TM norm-conserving pseudopotentials and local density approximation (LDA) exchange-correlation functional to evaluate the Bloch states and the phonon perturbation potentials. The kinetic energy cutoff was tested to choose 100 Ry. A Γ-centered Brillouin-zone mesh of $24\times24\times24$ mesh was employed to calculate charge density. The phonon was calculated on a Γ-centered $6\times6\times6$ mesh. Maximally localized Wannier functions (MLWF) were constructed on a $6\times6\times6$ grid of the Brillouin zone with the $1s$, $2s$, and $3s$ $3p$ orbitals for H, Mg, and Si, respectively. Fine electron ($60\times60\times60$) and phonon ($30\times30\times30$) grids were interpolated into the EPC constant with the Wannier90 [37] and EPW (electron-phonon coupling using Wannier functions) [38] codes.

III. RESULTS AND DISCUSSION

A. Determination of stable stoichiometries and divergent synthesis routes

Different from the binary system, there are some potential difficulties in predicting the stable stoichiometries of ternary hydrides. Above all, we have to consider a great deal of stoichiometries to construct a convex hull and then choose stable structures. However, obviously it is unrealistic to get all stable Mg-Si-H stoichiometries. In order to reduce computational costs and attain precise search ranges, we used the variable-composition prediction method by taking into account a little bit of Mg, Si, but massive H. For each stoichiometry, the maximum atomic numbers of every species were restricted to less than 4 for magnesium (Mg), 4 for silicon (Si), and 16 for hydrogen (H), which means total stoichiometries are 403, including 256 trihydrides, 128 binary hydrides, 16 Mg-Si alloys, and the rest 3 elements (i.e., Mg, Si, and H). Treating Mg, Si, and H as fundamental search blocks, we undertook the variable-composition predictions and the generalized trigonal high-pressure phase diagrams are depicted in Fig. 1. Although the initial searching pressure is 50 GPa, Fig. 1 is constructed from 200 GPa, because the dynamically unstable or nonmetallic feature for these three phases (R-3m, Pm-3, and $C2/m$) of $MgSiH_6$ are below 200 GPa, which will be discussed later.

As is shown in Fig. 1, for elemental solids located on three vertexes of triangle, we predicted a bcc Mg, a fcc Si, and a $C2/c$ H from 200 to 300 GPa, in excellent agreement with previous reports [39–41]. For a binary system, we predicted eight different stoichiometries located on three sides (Mg-H, Si-H, and Mg-Si) of a triangle, i.e., $P6_3/mmc$-MgH_2, $Cmcm$-MgH_4, R-3-MgH_{12}, P-1-MgH_{16},SiH_4, Fm-3m-Mg_3Si, $P6/mmm$-Mg_2Si, and $P4/mmm$-MgSi. These predicted binary Mg-H system compounds (see a more detailed Fig. S1 in the Supplemental Materials (SM) [42]) are in accord with literature [43]. Silane (SiH_4) falls on the Si-H side and its high-pressure phase is consistent with that in literature [10]. For the Mg-Si system, at ambient pressure, Mg_2Si is the only stable compound [44]. In this Mg-Si-O system [23], $P6/mmm$-Mg_2Si was reported to be the only stable binary compound above 0.5 TPa. However, our predictions suggest that Mg_3Si, Mg_2Si, and MgSi are located on the Mg-Si side from 200 to 300 GPa (Fig. S2 [42]) and their crystal structure information can be found in the SM [42] (Fig. S3 and Table S1). Furthermore, calculations on thermodynamics, mechanics, and dynamics demonstrate that they are stable (Table S2 and Fig. S4 [42]). All of these reported stable elemental solids and binary compounds on three vertexes and sides of triangles, respectively, were also found in our work, demonstrating that our results are credible and these chemical species are suitable as high-pressure reactants.

Except for elemental solids and binary compounds, we predicted seven ternary hydrides Mg_3SiH, $MgSiH$, $MgSiH_2$, $MgSiH_3$, $MgSiH_4$, $MgSiH_6$, and Mg_2SiH_8 from 200 to 300 GPa located inside of the triangle depicted in Fig. 1, and their crystal structure information can be also found in Fig. S5 and Table S3 [42]. Obviously these ternary hydrides can be obtained by directly compressing Mg, Si, and H. Besides, others synthesis routes could exist to obtain ternary

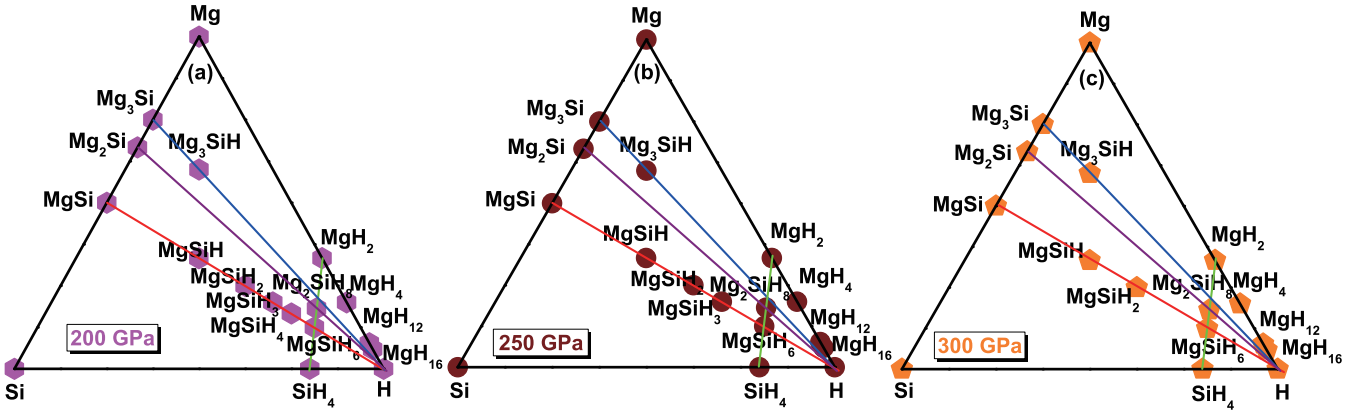

FIG. 1. Trigonal phase diagrams of the Mg-Si-H system at 200, 250, and 300 GPa, respectively. Solid symbols denote stable stoichiometries. Four different color lines stand for different synthesis routes for ternary hydrides.

hydrides due to abundant precursors (stable elemental solids and binary compounds). Some possible formation-route types for ternary hydrides can be summarized: A + B + C → D; A + B → D; A + B → D + E; A + B → D + E + F; A → B + C; A → B + C + D types, etc., where the left of the arrows is/are the reactant(s) and the resultant(s) are on the right.

In this work, the A + B → D type formation route is mainly concerned. Herein we propose a method to judge the specific synthesis pathways for ternary hydrides. Namely, if a straight line connected any two stable species A and B (elements or compounds) passes through another ternary hydride C, proving that the ternary hydride C might be synthesized by these two species A and B. We call this method the "triangle straight-line method" (TSLM). Based on this method, it can be clearly seen that Mg_3SiH is obtained by combining Mg_3Si alloy and elemental H (blue line in Fig. 1). $MgSiH_n$ ($n = 1, 2, 3, 4$) could be synthesized by combining MgSi alloy with different concentrations of hydrogen (red line in Fig. 1). Intriguingly, two different color lines (red and green) intersect at $MgSiH_6$, indicating that it could be synthetized by two substantially different synthesis routes, i.e., $MgH_2 + SiH_4 \rightarrow MgSiH_6$ and $MgSi + 3H_2 \rightarrow MgSiH_6$. Likewise, purple and green lines intersecting at Mg_2SiH_8 suggests that it could be also obtained via $2MgH_2 + SiH_4$ and $Mg_2Si + 4H_2$. We do emphasize that some other binary or ternary stoichiometries are possibly attained by extending the search range or adding atomic numbers, but it needs more computational costs.

To verify the reasonability of the above-mentioned TSLM, we performed fixed-composition predictions by considering five different stoichiometres (i.e., Mg_3SiH_{10}, Mg_2SiH_8, $MgSiH_6$, $MgSi_2H_{10}$, and $MgSi_3H_{14}$) with MgH_2 and SiH_4 treated as precursors. The enthalpies of formation for candidate stoichiometries with respect to dissociation into MgH_2 and SiH_4 at 200 to 300 GPa are calculated and depicted in Figs. 2(a)–2(c). It is found that both $MgSiH_6$ and Mg_2SiH_8 are located on tielines from 200 to 300 GPa, indicating they are thermodynamically stable and could be synthesized by mixing MgH_2 and SiH_4, proving that TSLM is an effective method to determine the specific synthesis route for ternary hydrides of the Mg-Si-H system. Owing to the most negative formation enthalpies, $MgSiH_6$ can be synthesized more easily than Mg_2SiH_8 in principle. Mg_3SiH_{10}, $MgSi_2H_{10}$, and $MgSi_3H_{14}$ are off the tielines, indicating they are thermodynamically unstable.

In addition, we carried out another fixed-composition prediction to verify the TSLM by taking into account eight different stoichiometres (i.e., MgSiH, $MgSiH_2$, $MgSiH_3$, $MgSiH_4$, $MgSiH_5$, $MgSiH_6$, $MgSiH_7$, and $MgSiH_8$) with respect to decomposition into MgSi alloy and elemental H. As depicted in Fig. 2(d), except for $MgSiH_5$, $MgSiH_7$, and $MgSiH_8$, other stoichiometries fall on the convex hull at 200 GPa. With increasing pressure, $MgSiH_4$ deviates distinctly the tieline and becomes unstable at 250 GPa shown in Fig. 2(e). Further compressed to 300 GPa [Fig. 2(f)], $MgSiH_3$ separates from the tieline. Notably, in the process of pressurization, $MgSiH_6$ is always on the convex hull, indicating it remains thermodynamically stable from 200 to 300 GPa. The above results show that MgSi can combine with one, two, three, four, and six H atoms at different pressures to form ternary MgSiH, $MgSiH_2$, $MgSiH_3$, $MgSiH_4$, and $MgSiH_6$, respectively, demonstrating that our TSLM is reasonable.

Herein it can be found that the TSLM is very useful in determining A + B → D type high-pressure formation routes for ternary hydrides of the Mg-Si-H system. It might be also applicable to all ternary compounds, which is very significant and helpful for further experimental synthesis. Notably, there may exist other pathways to obtain ternary $MgSiH_6$, such as the A + B + C → $MgSiH_6$ type listed in Table S4 (SM [42]), and others ternary compounds Mg_3SiH, MgSiH, $MgSiH_2$, $MgSiH_3$, $MgSiH_4$, and Mg_2SiH_8 might also exhibit some excellent properties (include superconductivity) at stable pressures, but these exceed our discussion scope.

B. Structural characteristics and electronic properties of cubic $MgSiH_6$

For $MgSiH_6$, three energetically competing phases R-3, $C2/m$, and Pm-3 were found via our structural predictions. The crystal structures and lattice parameters of R-3, $C2/m$, and Pm-3 $MgSiH_6$ are shown in Fig. S6 and Table S5 [42], respectively. Without considering zero-point energy (ZPE), we found that the R-3 phase is thermodynamically more stable than the other two phases below 113 GPa (Fig. 3). But the R-3 phase is dynamically unstable (Fig. S7). Above

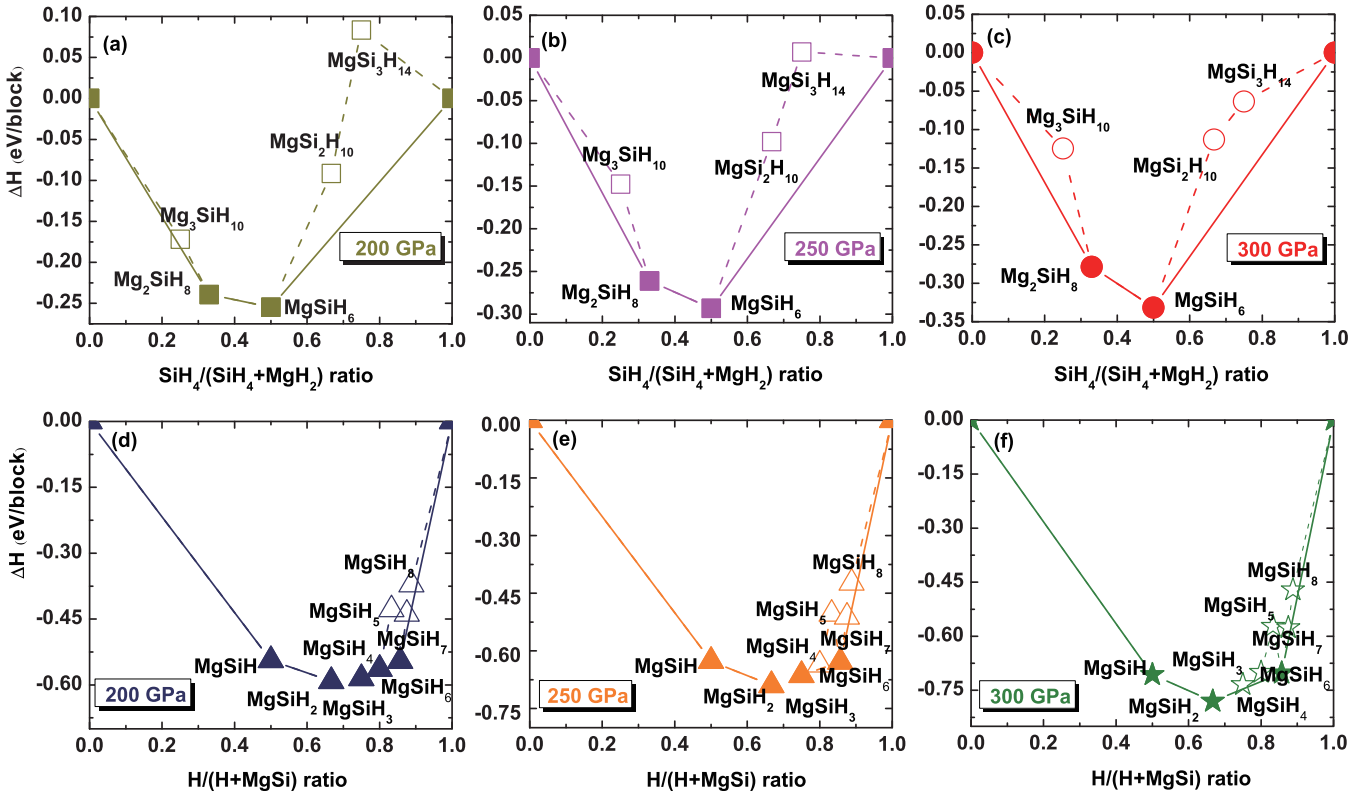

FIG. 2. (a)–(c) The formation enthalpies of Mg-Si-H compounds with respect to decomposition into MgH_2 and SiH_4 at different pressures. (d)–(f) The enthalpies of formation with respect to decomposition into MgSi alloy and H at different pressures. These solid lines stand for the convex hull, and solid symbols located on the convex hull represent stable stoichiometries. Open symbols connected by dashed lines indicate unstable species.

113 GPa, $C2/m$ phase becomes the more stable phase until 275 GPa, then it transforms to Pm-3 phase. The $C2/m$ phase exhibits a nonmetallic feature until the highest pressure 275 GPa (Fig. S8).

It can be also noted that the enthalpy of the $C2/m$ phase (23.96522 eV/f.u) is slightly lower than that of the Pm-3 phase (24.00464 eV/f.u) at 250 GPa, as listed in Table S6. However, it is well known that the zero-point energy (ZPE) is essential in determining structural stability of hydrogen-rich compounds, especially for where the energy difference between phases is very small. The ZPE can be defined as

$$E_{\mathrm{ZPE}} = \frac{1}{2}\sum_{q,v}\hbar\omega_{q,v}, \tag{1}$$

where v indicates a phonon branch at wave vector q and $\omega_{q,v}$ is the frequency at wave vector q in the zone. In formula (1), E_{ZPE} is proportional to $\omega_{q,v}$, which means some soft phonon modes (to be discussed in Sec. III C) might induce a lower E_{ZPE}. Since the Pm-3 phase is dynamically unstable at 200 GPa (Fig. S9), we calculated its ZPE from 250 GPa. The calculated ZPE of Pm-3 phase (2.13403 eV/f.u) is lower than that of $C2/m$ (2.35285 eV/f.u) at 250 GPa (see Table S6). Once the ZPE is included, the total energy of the Pm-3 phase become lower than that of the $C2/m$ phase from 250 to 300 GPa (inset of Fig. 3), meaning Pm-3 is more stable than $C2/m$ at this pressure range. Obviously, ZPE essentially lowers the stable pressure of Pm-3 $MgSiH_6$ at least 250 GPa or even lower. Therefore, it can be found that phonon softening affects the ZPE, and further reduces the pressure points of phase transition between competing $C2/m$ and Pm-3 phases.

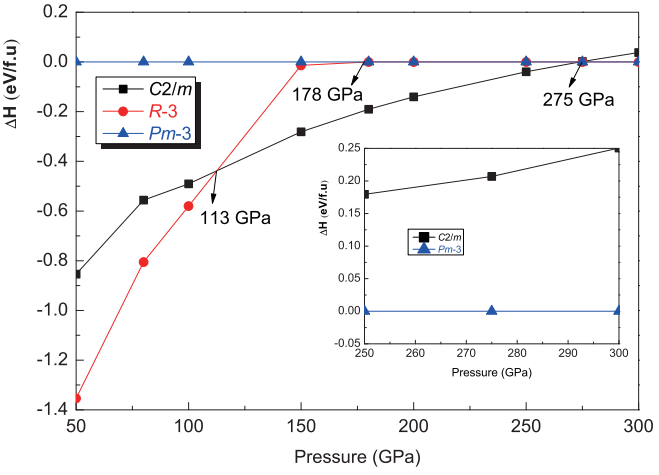

FIG. 3. The enthalpies per formula unit of R-3 and $C2/m$ phases as a function of pressure, referenced to Pm-3 phase of $MgSiH_6$. Illustration: The enthalpies of R-3 and $C2/m$ relative to Pm-3 phase with the zero-point motion corrections from 250 to 300 GPa.

Divergent synthesis routes produce the same $MgSiH_6$ adopting a simple cubic structure with group space Pm-3 at 250 GPa. As is depicted in Fig. 4(a), in cubic $MgSiH_6$, the

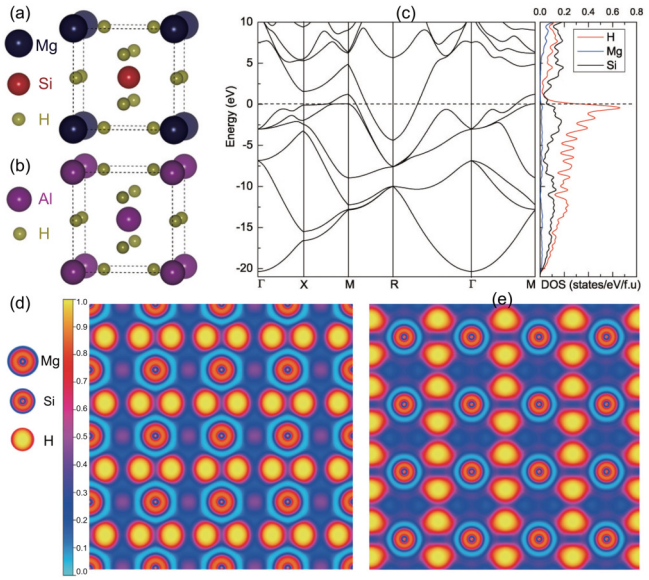

FIG. 4. (a), (c), (d), and (e) Some perspectives of Pm-3 $MgSiH_6$ at 250 GPa. (a) Crystal structure. The lattice parameters are $a = 2.851$ Å with H at 6g (0.255, 0.500, 0.00), Mg at 1b (0.500, 0.500, 0.500), and Si at 1a (0.000, 0.000, 0.000). (b) Crystal structure of Pm-3n AlH_3. (c) The electronic band structure and density of electronic states (DOS) of $MgSiH_6$. The electron localization function (ELF) of Mg-H (d) and Si-H (e) planes.

center and vertex of the simple cubic lattice are occupied by Si and Mg atoms, respectively. Moreover, all equivalent H atoms form chains arranged along the directions of axis. This structure is extremely similar to the binary A15-type hydride AlH_3 [45] [Fig. 4(b)]. The structural similarity can be explained from an alternative perspective by analyzing elemental mass and Pauling electronegativity. From the vibrational view, the atomic mass (M) is an anticipated major factor in the dynamic equation, and corresponding values of Mg, Al, and Si are 24.31, 26.98, and 28.09 a.m.u., respectively. Obviously, two M_{Al} is closed to $M_{Mg} + M_{Si}$, which could somewhat guarantee the dynamical stability of the system by replacing two Al atoms with Mg and Si atoms. By analysis of Pauling electronegativity, we found that the effect of two Al atoms can be completely displaced by Mg + Si, because the electronegativity of Al is closed to a half of Mg + Si. More importantly, in Pm-3n Al_2H_6 (AlH_3 can be written as Al_2H_6), all H atoms form a sublattice and two Al atoms provide six electrons to stabilize the structural framework. In a similar H sublattice of Pm-3 $MgSiH_6$, Mg and Si replace two Al to offer the same amount of electrons.

The electronic band structure and density of electronic states (DOS) of $MgSiH_6$ at 250 GPa are calculated and shown in Fig. 4(c). The energy band structure characterizes the metallic character with bands overlapping at Fermi level. It is clearly seen that a steep conduction band crosses the Fermi level along Γ-R-M direction and forms an "electron pocket" around R points. Simultaneously, two flat valence bands appear in the vicinity of Fermi level along X-M direction. The "flat band–steep band" concurrently occurring in $MgSiH_6$ indicates that it may be a good high temperature superconductor [46]. Although $MgSiH_6$ takes on a similar crystalline structure with AlH_3, the band structure dependence

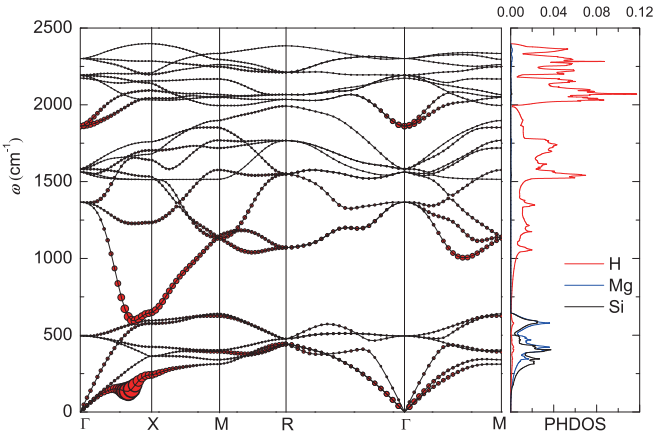

FIG. 5. Phonon band structure (a) and projected density of states (PHDOS) (b) of Pm-3 $MgSiH_6$ at 250 GPa. These red solid circles with black borders overlapping with band show mode-resolved electron phonon coupling constants $\lambda_{q,v}$ and the sizes of the circles are proportional to EPC strength.

on pressure is essentially different from that of AlH_3. The band structures of $MgSiH_6$ are not dramatically changed from 250 to 300 GPa. However, with increasing pressures, AlH_3 exhibits an antimetallization behavior [47]. Besides, it can be found that H atoms provide significant contributions to DOS at Fermi level $N(\varepsilon_F)$, which is very similar with some binary hydrogen-dominated high-T_c superconductors [4]. High $N(\varepsilon_F)$ usually means a large EPC strength [48]. Figures 4(d) and 4(e) show the electron localization function (ELF) of $MgSiH_6$ and no electron localization is found between Mg-H and Si-H, indicating the ionic nature of the system. Note that there are no molecular units in $MgSiH_6$, which is different from the CH_4 units contained in $MgCH_4$ [9].

C. Phonon softening, Fermi surface nesting, and superconductivity

To ensure the structural stability of $MgSiH_6$ at high pressure, the mechanics and the lattice dynamics were tested at 250 GPa. The strain energy of a mechanically stable crystal must be positive, namely, the matrix of elastic constants (C_{ij}) should be positive. The simple mechanical stability criteria of a cubic phase is given by $C_{11} > 0$, $C_{44} > 0$, $C_{11} > |C_{12}|$, and $(C_{11} + 2C_{12}) > 0$ [49]. In the cubic phase of $MgSiH_6$, the $C_{11} = 777.98$, $C_{44} = 226.1$, and $C_{12} = 432.8$ GPa, and they satisfy mechanical stability criteria, demonstrating $MgSiH_6$ is mechanically stable at 250 GPa. The phonon band structure and the projected density of states (PHDOS) at 250 GPa is depicted in Fig. 5. The presence of no imaginary frequency in the phonon spectra indicates the dynamical stability of the cubic phase [Fig. 5(a)]. Owing to the discrepancy of atomic mass, these vibrational modes can be divided into two major regions. As is depicted in Fig. 5(b), the low-frequency vibrational modes below about 645 cm^{-1} are dominated by heavier Mg and Si atoms, and the high-frequency region is mainly associated with H atomic vibration modes. It is found that the positions and values of peaks in PHDOS derived from Mg and Si atoms are very similar, which is ascribed to similar atomic masses and positions.

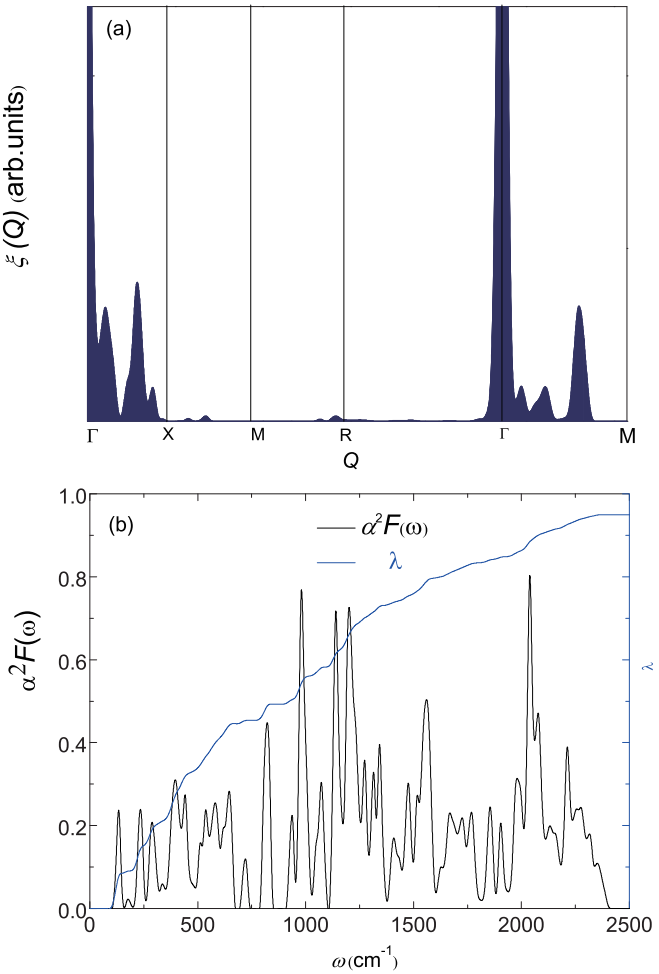

FIG. 6. Some planes for $MgSiH_6$ at 250 GPa. (a) The calculated nesting function $\xi(Q)$ along some special Q trajectories. The calculation employs 5225 k points and 658350 $k+Q$ points to attain their respective energy eigenvalues. (b) The Eliashberg phonon spectral function $\alpha^2F(\omega)$ and the electron-phonon integral λ.

A prominent feature in the phonon dispersion is the presence of soft phonon modes mainly concentrated in two regions. The lowest acoustic vibration mode (branch 1) undergoes softening along Γ-X and the seventh vibration mode softens along Γ-X and Γ-M [Fig. 5(a)]. To clearly elucidate this reason of phonon softening, we investigated the Fermi surface nesting in the cubic $MgSiH_6$ by applying the nesting function

$$\xi(Q) = \frac{1}{N}\sum_{\vec{k},i,j}\delta(\varepsilon_{\vec{k},i}-\varepsilon_F)\delta(\varepsilon_{\vec{k}+\vec{Q},j}-\varepsilon_F), \qquad (2)$$

where $\varepsilon_{k,i}$ is the Kohn-Sham eigenvalue and i, j are the indices of energy bands, N is the number of k points, and ε_F is the Fermi energy. To calculate the $\xi(Q)$, we used the density function of normal distribution (i.e., Gaussian function) to replace the δ function with broadening of 0.01. The large value of nesting function $\xi(Q)$ for a vector Q vividly describes high probability for parallel portions of the Fermi surface nested by a Q. Figure 6(a) shows the $\xi(Q)$ along high-symmetry lines Γ-X-M-R-Γ-M. For Γ point, its $\xi(Q)$ represents the entire Fermi surface nests into itself, which has no actual physical meaning. The $\xi(Q)$ quantitatively describes two

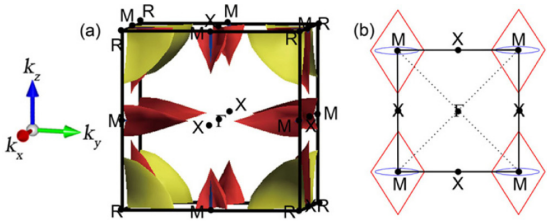

FIG. 7. Fermi surface for $MgSiH_6$ at 250 GPa. (a) Three-dimensional (3D) Fermi surface calculated with 60×60×60 k mesh. (b) 2D Fermi surface along Γ-X and Γ-M directions calculated with 216 000 k points. The solid line represents the boundary of first Brillouin zone and possible nesting vectors in (b) are indicated by dashed lines.

sharp peaks along Γ-X and Γ-M directions, demonstrating that strong Fermi surface nesting occurs at these directions. Not coincidentally, it can be observed from Fig. 5(a) that the regions of phonon softening correspond to the nesting directions, strongly indicating phonon softening is induced by Fermi surface nesting. Furthermore, this quantitative calculation on $\xi(Q)$ can be proved by observing the contour of the Fermi surface, as depicted in Fig. 7. Peaks in $\xi(Q)$ along Γ-X direction are related to nesting vectors along the k_x, k_y, and k_z axes [Fig. 7(a)]. Peaks along Γ-M direction correspond to the obvious Fermi surface nesting depicted in Fig. 7(b).

To explore the superconductivity of $MgSiH_6$, we investigated the EPC parameter λ in two ways. Based on density functional perturbation theory (DFPT), we used QE with the coarse 6×6×6 q mesh and obtained the $\lambda = 0.956$ at 250 GPa. In order to attain the more precise EPC parameter λ, the more accurate electron-phonon interaction matrix elements depending on the number of k and q points should be calculated with denser k mesh and q mesh. Therefore, the EPW was used to compute λ with fairly dense k mesh (60×60×60) and q mesh (30×30×30) (see Sec. II). Nonetheless, we found the value of λ from the EPW calculation is 0.943, which is close to that from QE, indicating both ways are reasonable in estimating EPC. Calculation reveals a large $\lambda = 0.96$ or 0.94, suggesting the electron phonon coupling is fairly strong.

The spectral function $\alpha^2F(\omega)$ and the integrated EPC parameter λ as a function of frequency are shown in Fig. 6(b). It is found that the low-frequency and high-frequency contribute 45% and 55% to total EPC λ, respectively. Herein, it is noted that the low frequency provides very important contributions to EPC, which is significantly different from some binary H_2 units containing hydrides [11,12,50–52] and recently fashionable H_3S [1]. As will be discussed later, the important difference is a relation with soft phonons of low frequency. The superconducting critical temperature T_c can be evaluated by using the Allen-Dynes modified McMillan equation [53]

$$T_c = \frac{\omega_{\log}}{1.2}\exp\left[-\frac{1.04(1+\lambda)}{\lambda-\mu^*(1+0.62\lambda)}\right], \qquad (3)$$

where Coulomb pseudopotential μ^* with 0.10–0.13 is appropriate for hydrogen-rich compounds. For $\lambda < 1.5$, this equation can provide a highly accurate value of T_c. As is listed in Table S7 [42], using the calculated $\lambda = 0.96$ and the logarithmically averaged phonon frequency $\omega_{\log} = 973.81$ K, we predicted the T_c of $MgSiH_6$ to reach a high value 53–63 K

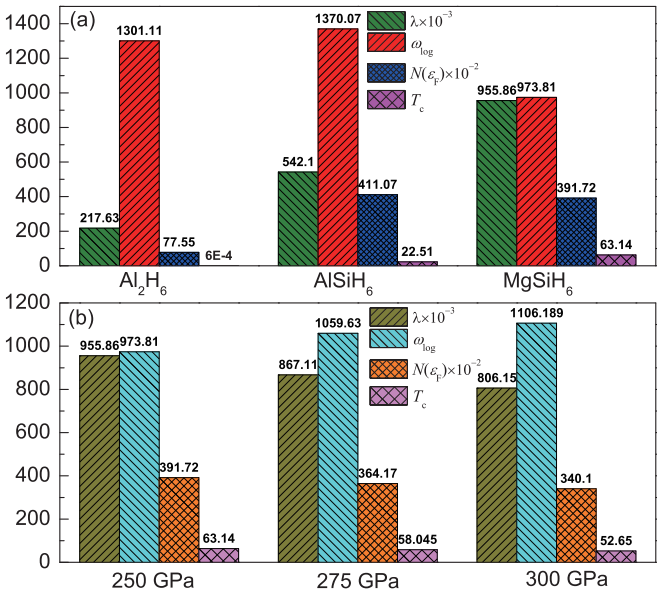

FIG. 8. (a) EPC parameter (λ), the phonon frequency logarithmic average ($\omega_{\log}$) in Kelvin (K), the electronic DOS at Fermi level $N(\varepsilon_F)$ in states/spin/Ry/cell, and superconducting transition temperature $T_c(\mu^* = 0.1)$ in Kelvin (K) for Pm-3n Al_2H_6, Pm-3 $AlSiH_6$, and Pm-3 $MgSiH_6$ at 250 GPa. (b) The pressure evolution of λ, $\omega_{\log}$, $N(\varepsilon_F)$, and $T_c(\mu^* = 0.1)$ for $MgSiH_6$ at selected pressures.

with $\mu^* = 0.10$–0.13 at 250 GPa. The T_c is relatively high in those reported ternary hydrides.

To explore the dependence of the superconductivity on soft phonon modes, we extend calculations on two aspects. On one hand, we calculated these mode-resolved electron phonon coupling constants $\lambda_{q,v}$ projected on phonon spectra, as depicted in Fig. 5(a). $\lambda_{q,v}$ is the weight function to evaluate overall EPC parameter λ which can be expressed as

$$\lambda = \sum_{q,v} \lambda_{q,v} w_{q,v}, \tag{4}$$

where q, v are phonon vector and the index of mode, respectively, and $w_{q,v}$ is the weight of each q point in the first Brillouin zone (BZ). It is clearly seen that $\lambda_{q,v}$ is particularly enhanced in these regions of phonon softening [Fig. 5(a)], suggesting soft phonon modes boost the EPC strength, which explains why the low frequency provides important contributions to EPC. On the other hand, we performed a calculation on the evolution of superconductivity by simulating Al_2H_6 (AlH_3) to be gradually substituted to $MgSiH_6$ at 250 GPa. In order to ensure the stability of structure, we used a Si atom to replace an Al atom to form the Pm-3 $AlSiH_6$. Subsequently, the other Al atom is substituted by the Mg atom to form the Pm-3 $MgSiH_6$. For three high-pressure crystal structures (i.e., Pm-3n Al_2H_6, Pm-3 $AlSiH_6$, and Pm-3 $MgSiH_6$) at 250 GPa, they are dynamically stable without displaying any negative frequency (see Figs. S10 and S11 [42]). Besides, for Al_2H_6 and $AlSiH_6$, no phonon softening is observed in phonon spectra. Figure 8(a) shows some crucial parameters involved with superconductivity. The electronic DOS at Fermi level $N(\varepsilon_F)$ of $MgSiH_6$ (3.91 states/spin/Ry/cell) is comparable with that of isostructural $AlSiH_6$ (4.11 states/spin/Ry/cell). However, owing to these soft phonon modes, the EPC strength of $MgSiH_6$ ($\lambda = 0.96$) is obviously larger than that of $AlSiH_6$ ($\lambda = 0.54$). Contrary, soft phonon modes render $MgSiH_6$ to produce the lower $\omega_{\log}$ (973.81 K) than those of Al_2H_6 (1301.11 K) and $AlSiH_6$ (1370.07 K). Therefore, it can be summarized that soft phonon modes synchronously play two opposite roles in predicting the superconductivity. On one aspect, phonon softening does boost the EPC strength. However, on the other aspect, these soft phonon modes evidently suppress the $\omega_{\log}$. In the Allen-Dynes modified McMillan equation, T_c is the balanced results of λ and $\omega_{\log}$. Figure 8(b) shows the pressure evolution of some important parameters involved with the superconductivity of $MgSiH_6$. It is clearly seen that, as a consequence of pressurization, the phonon tends to harden and $\omega_{\log}$ raises, but the EPC parameter λ decreases. The reduction of T_c indicates that the λ dominates the superconductivity. It is very obvious that $MgSiH_6$ is a phonon-mediated high temperature superconductor and T_c has a weak dependence on pressure with a coefficient (dT_c/dP) of -0.21 K/GPa.

IV. CONCLUSION

In summary, we performed first-principles calculations to investigate the high-pressure crystal structures and superconductivity of the Mg-Si-H system. We put forward a method to determine the specific synthesis routes of ternary hydrides. This method reveals that the stoichiometric $MgSiH_6$ can be obtained by two different A + B $\rightarrow$ D formation ways at high pressure: $MgH_2 + SiH_4 \rightarrow MgSiH_6$ and $MgSi + 3H_2 \rightarrow MgSiH_6$. $MgSiH_6$ exhibits a Pm-3 symmetry and primary ionic feature, which was predicted to possess a large EPC parameter and high superconducting transition temperature of 63 K at 250 GPa. Soft phonon modes induced by the Fermi surface nesting have been found to be very effective in enhancing the EPC, playing an important role in superconductivity. Our work suggests that high temperature superconductivity can be achieved in ternary hydrides under high pressures. The current work could provide helpful and clear guidance for further experimental synthesis for ternary hydrides under high pressure.

ACKNOWLEDGMENTS

Dedicated to Professor Guangtian Zou on the occasion of his 80th birthday. This work was supported by the National Natural Science Foundation of China (No. 51632002, No. 51572108, No. 11674122, No. 11634004, No. 11504127, No. 11574109, and No. 11404134), Program for Changjiang Scholars and Innovative Research Team in University (No. IRT_15R23), the 111 Project (No. B12011), National Found for Fostering Talents of basic Science (No. J1103202), and Jilin Provincial Science and Technology Development Project of China (20170520116JH). Work at Carnegie was supported by EFree, an Energy Frontier Research Center funded by the DOE, Office of Science, Basic Energy Sciences under Award No. DE-SC-0001057. Parts of the calculations were performed in the High Performance Computing Center (HPCC) of Jilin University and TianHe-1(A) at the National Supercomputer Center in Tianjin.

[1] D. Duan, Y. Liu, F. Tian, D. Li, X. Huang, Z. Zhao, H. Yu, B. Liu, W. Tian, and T. Cui, Sci. Rep. **4**, 6968 (2014).

[2] A. P. Drozdov, M. I. Eremets, I. A. Troyan, V. Ksenofontov, and S. I. Shylin, Nature (Londo) **525**, 73 (2015).

[3] M. Einaga, M. Sakata, T. Ishikawa, K. Shimizu, M. I. Eremets, A. P. Drozdov, I. A. Troyan, N. Hirao, and Y. Ohishi, Nat. Phys. **12**, 835 (2016).

[4] D. Duan, Y. Liu, Y. Ma, Z. Shao, B. Liu, and T. Cui, Natl. Sci. Rev. **4**, 121 (2017).

[5] N. W. Ashcroft, Phys. Rev. Lett. **92**, 187002 (2004).

[6] T. Muramatsu, W. K. Wanene, M. Somayazulu, E. Vinitsky, D. Chandra, T. A. Strobel, V. V. Struzhkin, and R. J. Hemley, J. Phys. Chem. C **119**, 18007 (2015).

[7] S. Zhang, L. Zhu, H. Liu, and G. Yang, Inorg. Chem. **55**, 11434 (2016).

[8] M. Rahm, R. Hoffmann, and N. W. Ashcroft, J. Am. Chem. Soc. **139**, 8740 (2017).

[9] F. Tian, D. Li, D. Duan, X. Sha, Y. Liu, T. Yang, B. Liu, and T. Cui, Mater. Res. Express **2**, 046001 (2015).

[10] M. I. Eremets, I. A. Trojan, S. A. Medvedev, J. S. Tse, and Y. Yao, Science **319**, 1506 (2008).

[11] G. Gao, A. R. Oganov, A. Bergara, M. Martinez-Canales, T. Cui, T. Iitaka, Y. Ma, and G. Zou, Phys. Rev. Lett. **101**, 107002 (2008).

[12] J. S. Tse, Y. Yao, and K. Tanaka, Phys. Rev. Lett. **98**, 117004 (2007).

[13] V. V. Struzhkin, D. Y. Kim, E. Stavrou, T. Muramatsu, H.-k. Mao, C. J. Pickard, R. J. Needs, V. B. Prakapenka, and A. F. Goncharov, Nat. Commun. **7**, 12267 (2016).

[14] D. Duan, X. Huang, F. Tian, D. Li, H. Yu, Y. Liu, Y. Ma, B. Liu, and T. Cui, Phys. Rev. B **91**, 180502 (2015).

[15] T. A. Strobel, P. Ganesh, M. Somayazulu, P. R. C. Kent, and R. J. Hemley, Phys. Rev. Lett. **107**, 255503 (2011).

[16] N. Bernstein, C. S. Hellberg, M. D. Johannes, I. I. Mazin, and M. J. Mehl, Phys. Rev. B **91**, 060511 (2015).

[17] I. Errea, M. Calandra, C. J. Pickard, J. Nelson, R. J. Needs, Y. Li, H. Liu, Y. Zhang, Y. Ma, and F. Mauri, Phys. Rev. Lett. **114**, 157004 (2015).

[18] A. F. Goncharov, S. S. Lobanov, V. B. Prakapenka, and E. Greenberg, Phys. Rev. B **95**, 140101 (2017).

[19] A. R. Oganov, A. O. Lyakhov, and M. Valle, Acc. Chem. Res. **44**, 227 (2011).

[20] A. O. Lyakhov, A. R. Oganov, H. T. Stokes, and Q. Zhu, Comput. Phys. Commun. **184**, 1172 (2013).

[21] Y. Wang, J. Lv, L. Zhu, and Y. Ma, Phys. Rev. B **82**, 094116 (2010).

[22] Y. Wang, J. Lv, L. Zhu, and Y. Ma, Comput. Phys. Commun. **183**, 2063 (2012).

[23] H. Niu, A. R. Oganov, X.-Q. Chen, and D. Li, Sci. Rep. **5**, 18347 (2015).

[24] G. Saleh and A. R. Oganov, Sci. Rep. **6**, 32486 (2016).

[25] S. Wang, A. R. Oganov, G. Qian, Q. Zhu, H. Dong, X. Dong, and M. M. Davari Esfahani, Phys. Chem. Chem. Phys. **18**, 1859 (2016).

[26] G. Kresse and D. Joubert, Phys. Rev. B **59**, 1758 (1999).

[27] G. Kresse and J. Furthmüller, Phys. Rev. B **54**, 11169 (1996).

[28] J. P. Perdew, K. Burke, and M. Ernzerhof, Phys. Rev. Lett. **77**, 3865 (1996).

[29] A. Togo, F. Oba, and I. Tanaka, Phys. Rev. B **78**, 134106 (2008).

[30] S. Baroni, S. de Gironcoli, A. Dal Corso, and P. Giannozzi, Rev. Mod. Phys. **73**, 515 (2001).

[31] P. Giannozzi, S. Baroni, N. Bonini, M. Calandra, R. Car, C. Cavazzoni, D. Ceresoli, G. L. Chiarotti, M. Cococcioni, I. Dabo, A. Dal Corso, S. de Gironcoli, S. Fabris, G. Fratesi, R. Gebauer, U. Gerstmann, C. Gougoussis, A. Kokalj, M. Lazzeri, L. Martin-Samos, N. Marzari, F. Mauri, R. Mazzarello, S. Paolini, A. Pasquarello, L. Paulatto, C. Sbraccia, S. Scandolo, G. Sclauzero, A. P. Seitsonen, A. Smogunov, P. Umari, and R. M. Wentzcovitch, J. Phys.: Condens. Matter **21**, 395502 (2009).

[32] N. Troullier and J. L. Martins, Phys. Rev. B **43**, 1993 (1991).

[33] F. Giustino, J. R. Yates, I. Souza, M. L. Cohen, and S. G. Louie, Phys. Rev. Lett. **98**, 047005 (2007).

[34] T. Bazhirov, Y. Sakai, S. Saito, and M. L. Cohen, Phys. Rev. B **89**, 045136 (2014).

[35] T. Bazhirov, J. Noffsinger, and M. L. Cohen, Phys. Rev. B **82**, 184509 (2010).

[36] I. Souza, N. Marzari, and D. Vanderbilt, Phys. Rev. B **65**, 035109 (2001).

[37] A. A. Mostofi, J. R. Yates, Y.-S. Lee, I. Souza, D. Vanderbilt, and N. Marzari, Comput. Phys. Commun. **178**, 685 (2008).

[38] J. Noffsinger, F. Giustino, B. D. Malone, C.-H. Park, S. G. Louie, and M. L. Cohen, Comput. Phys. Commun. **181**, 2140 (2010).

[39] P. Li, G. Gao, Y. Wang, and Y. Ma, J. Phys. Chem. C **114**, 21745 (2010).

[40] H. Katzke, U. Bismayer, and P. Tolédano, Phys. Rev. B **73**, 134105 (2006).

[41] C. J. Pickard and R. J. Needs, Nat. Phys. **3**, 473 (2007).

[42] See Supplemental Material at http://link.aps.org/supplemental/10.1103/PhysRevB.96.144518 for brief description of materials.

[43] D. C. Lonie, J. Hooper, B. Altintas, and E. Zurek, Phys. Rev. B **87**, 054107 (2013).

[44] X.-Y. Yan, Y. A. Chang, and F. Zhang, J. Phase Equilib. **21**, 379 (2000).

[45] C. J. Pickard and R. J. Needs, Phys. Rev. B **76**, 144114 (2007).

[46] A. Simon, Angew. Chem., Int. Ed. **36**, 1788 (1997).

[47] M. Geshi and T. Fukazawa, Physica B **411**, 154 (2013).

[48] F. Peng, Y. Sun, C. J. Pickard, R. J. Needs, Q. Wu, and Y. Ma, Phys. Rev. Lett. **119**, 107001 (2017).

[49] Z. J. Wu, E. J. Zhao, H. P. Xiang, X. F. Hao, X. J. Liu, and J. Meng, Phys. Rev. B **76**, 054115 (2007).

[50] G. Gao, A. R. Oganov, P. Li, Z. Li, H. Wang, T. Cui, Y. Ma, A. Bergara, A. O. Lyakhov, T. Iitaka, and G. Zou, Proc. Natl. Acad. Sci. USA **107**, 1317 (2010).

[51] X. Zhong, H. Wang, J. Zhang, H. Liu, S. Zhang, H.-F. Song, G. Yang, L. Zhang, and Y. Ma, Phys. Rev. Lett. **116**, 057002 (2016).

[52] Y. Liu, D. Duan, F. Tian, C. Wang, G. Wu, Y. Ma, H. Yu, D. Li, B. Liu, and T. Cui, RSC Adv. **5**, 103445 (2015).

[53] P. B. Allen and R. C. Dynes, Phys. Rev. B **12**, 905 (1975).